

## Heat transfer area optimization of intermediate heat-exchange cycle system for aero engines



Yanchen Fu <sup>a,b,c,d</sup>, Weitong Liu <sup>a,b,c,d</sup>, Han Qi <sup>b,c,d</sup>, Qun Chen <sup>e</sup>, Jie Wen <sup>a,b,c,d</sup>, Guoqiang Xu <sup>a,b,c,d,\*</sup>

<sup>a</sup> Research Institute of Aero-engine, Beihang University, Beijing 100191, China

<sup>b</sup> National Key Laboratory of Science and Technology on Aero-Engine Aero-thermodynamics, Beihang University, Beijing 100191, China

<sup>c</sup> Frontiers Science Center for Super-cycle Aeroengine's Aerothermodynamics, Beihang University, Beijing 100191, China

<sup>d</sup> Collaborative Innovation Center for Advanced Aero-Engine, Beihang University, Beijing 100191, China

<sup>e</sup> Key Laboratory for Thermal Science and Power Engineering of Ministry of Education, Department of Engineering Mechanics, Tsinghua University, Beijing 100084, China

### ARTICLE INFO

#### Keywords:

heat transfer system  
heat transfer area  
heat exchanger  
aero engine  
cycle optimization

### ABSTRACT

The present study constructs an intermediate heat-exchange cycle system for aero engines. To explore the impact of circulation parameters on the cycle, a mathematical model has been developed. Based on the mathematical model, a novel and convenient approach to determining intermediate working fluid (IWF) mass flow rate and temperature, achieving the minimum total system heat transfer area, has been proposed. A two-stage heat exchanger combined intermediate heat-exchange cycle system with Chinese aviation kerosene RP-3, high-pressure water, and air as working fluids is taken as an example to verify the analytical results through numerical calculations. The deviation between the analytical and numerical results is relatively small, below 0.03%. For the situation of a given higher intermediate temperature, a wide range of IWF mass flow rates can be selected as the design point without significantly affecting the total heat transfer area. For the situation where both intermediate temperature and IWF mass flow rate are variable, an optimal area exists where the total heat transfer area is very low and does not differ much with each point. Overall, the present findings can serve as reasonably accurate preliminary guidelines for designing and optimizing the intermediate heat-exchange cycle system.

### 1. Introduction

A variety of techniques have been used in advanced aero engines to achieve high thrust-to-weight ratio, high stability, and low specific fuel consumption. The aero engine design heavily depends on the option of propulsion system among these technologies. For advanced supersonic vehicles, the propulsion system can be divided into three categories on the basis of the mechanism of engine combination: PTCC [1], TBCC [2], and RBCC [3]. Among them, PTCC is considered to be a promising alternative to raise the working Mach number with a wide speed range [4,5].

The existing PTCC schemes were categorized into four types by Wang et al. [1]: Fuel Precooling (FPC), Third Fluid Cooling (TFC), Mass Injection and Pre-compressor Cooling (MIPCC), and the combination of FPC and MIPCC. And a wide range of explorations have been conducted over the past decades to screen promising engine configurations. A

two-stage pre-cooler structure was first proposed by Webber et al. [6], who demonstrated that the utilization of a precooling caused significant thermodynamic irreversibility. However, the stability, security, and implementability of PTCC engines still need to be verified through considerable experiments. Since the thermal management system for the aero engine is particularly important, except for the PTCC engines, lots of researchers also put the spotlight on Cooled Cooling Air (CCA) technology which in both commercial and military engines shows more advantages than PTCC technology by modifying the corresponding cycle parameters rather than the cycling process [7].

CCA technology employs either inlet ram air, bypass stream air, or fuel to cool the compressor bleed air in order to meet the increasing thermal protection demands [8]. Compared with the use of inlet ram air or bypass stream air, using fuel as the coolant provides more advantages to the engine overall performance as below. 1. Compared to air, hydrocarbon fuel exhibits a higher heat sink capacity due to both sensible heating and endothermal heating from the chemical reaction [9]. 2.

\* Corresponding author.

E-mail address: [04822@buaa.edu.cn](mailto:04822@buaa.edu.cn) (G. Xu).

Nomenclature		
$A$	heat transfer area in the tube of each HEX [ $\text{m}^2$ ]	
$a$	constant	
$b$	constant	
$C_1$	constant	
$c_p$	isobaric specific heat capacity [ $\text{J/kg/K}$ ]	
$d_i$	tube inner diameter [mm]	
$d_o$	tube outer diameter [mm]	
$h_i$	heat transfer coefficient of the tube side [ $\text{W/m}^2/\text{K}$ ]	
$h_o$	heat transfer coefficient of the shell side [ $\text{W/m}^2/\text{K}$ ]	
$k_0$	thermal conductivity of the tube wall [ $\text{W/m/K}$ ]	
$L$	heat exchange unit tube lengths [m]	
$m_1$	mass flow rate of IWF [ $\text{kg/s}$ ]	
$m$	mass flow rate [ $\text{kg/s}$ ]	
$N_{tube}$	Number of heat exchange unit tubes	
$Nu$	Nusselt number	
$Pr$	Prandtl number	
$P$	pressure [MPa]	
$P_1$	pressure of IWF [MPa]	
$Q$	heat transfer rate [W]	
$Q_{equal}$	system equilibrium heat transfer rate [W]	
$R$	calculation coefficient	
$Re$	Reynolds number	
$T_1$	intermediate temperature [ $^\circ\text{C}$ ]	
$T_2$	the IWF outlet temperature of HEX-1 [ $^\circ\text{C}$ ]	
$T$	temperature [ $^\circ\text{C}$ ]	
$\Delta T_m$	mean temperature difference [ $^\circ\text{C}$ ]	
$U_o$	overall heat transfer coefficient [ $\text{W/m}^2/\text{K}$ ]	
Greek symbol		
$\alpha$	calculation coefficient	
		$\beta$ calculation coefficient
		$\sigma$ calculation coefficient
		$\mu$ dynamic viscosity [ $\mu\text{Pa}\cdot\text{s}$ ]
		<i>Subscript</i>
		1 HEX-1
		2 HEX-2
		<i>a</i> air
		<i>f</i> fuel
		<i>i</i> inlet
		<i>o</i> outlet
		<i>optimal</i> optimal
		<i>total</i> total
		<i>left</i> lower limit
		<i>right</i> upper limit
		<i>max</i> maximum
		<i>min</i> minimum
		<i>w</i> intermediate working fluid
		<i>Abbreviation</i>
		TBCC Turbine-based Combined Cycle
		RBCC Rocket-based Combined Cycle
		PTCC Precooled Turbine Combined Cycle
		CCA Cooled Cooling Air
		HEX Heat exchanger
		COP Coefficient of Performance
		IWF Intermediate working fluid
		LMTD Logarithmic Mean Temperature Difference
		AMTD Arithmetic Mean Temperature Difference
		GA Genetic Algorithm
		NaN Not a number

After absorbing the heat from the air, fuel temperature increases, resulting in an overall temperature rise of the combustion chamber that enhances engine performance. 3. As the fuel temperature and pressure are above their critical point, significant changes occur in the physical properties of the fuel, improving the combustion efficiency [10]. 4. The air-fuel heat exchanger (HEX) is more lightweight and compact than the air-air HEX in CCA systems [11]. Therefore, utilizing fuel as the heat sink offers more advantages than using air in CCA technology.

The literature on CCA technology is extensive and focuses particularly on the CCA system performance and the design of air-fuel CCA HEX. Miller [12] compared a turbojet cycle using the methane-air CCA technology with a reference cycle and pointed out there is a 1.2% reduction in specific thrust and a 1% reduction in specific impulse. Boyle and Jones [13] reported that precooling the turbine cooling air has a notable impact on reducing specific fuel consumption. However, a reduction in the cooling air temperature results in a decrease in the enthalpy of the cooling air. This reduction in enthalpy may have adverse consequences that surpass the advantages gained from precooling the turbine cooling air. To gain a comprehensive understanding of the costs and benefits of CCA technology, it is imperative to carefully examine the integration complexities and engine operation, as indicated by Gray et al. [14]. The investigation by Zhuang et al. [15] into the use of CCA technology in low bypass ratio aero engines revealed fluctuations in the performance of the CCA-HEX. Specifically, their findings demonstrated that heat transfer and flow resistance exhibit different characteristics at different altitudes and Mach numbers. Liu et al. [16] conducted a study aimed at reconciling the competing demands of power-to-weight ratio and air-side pressure drop in CCA technology. To achieve this goal, the researchers carried out a multi-objective optimization of air-fuel tube-in-tube helical coil HEXs.

Although these techniques are considered to be promising methods to achieve high Mach numbers, there are still lots of problems to be addressed. For PTCC engines, the aforementioned engines typically utilize the third fluid to transfer heat and thus form an intermediate heat-exchange cycle, which may significantly increase the engine weight. Moreover, most of these engines utilize liquid hydrogen for precooling fuel, which presents various safety and storage obstacles. For CCA technology, fuel coking and thermo-acoustic oscillations are major challenges for the fuel-cooled CCA HEXs [11,17]. Additionally, if there are processing problems with the fuel-air HEX structure, the fuel could potentially be exposed to the outside environment to trigger a fire. Thus, the primary research gap lies in identifying an efficient method to decrease the weight of the intermediate heat-exchange cycle and to utilize the fuel heat sink without the aforementioned issues.

The present study constructs an intermediate heat-exchange cycle system, and it can utilize the CCA technology without the potential safety hazard. Essentially, the built cycle is also the intermediate cycle subsystem of the PTCC engines. On one hand, it prevents to a certain extent the risk of engine fire caused by direct contact between fuel and high-temperature air due to HEX breakage by using a safe intermediate working fluid (IWF). On the other hand, for PTCC engines, using the IWF to precool the air can avoid the risk of blockage resulting from the coke formation of fuel in the precooling process. Therefore, investigating the characteristics of this cycle, especially the weight optimization, contributes to the development of CCA technology and PTCC engines.

Weight minimization of the HEXs within the intermediate heat-exchange cycle is crucial for the designer to minimize system size and achieve a high thrust-to-weight ratio. This holds even greater significance due to the relatively fixed specifications of other components like the circulating pump and accessories, which are determined by the

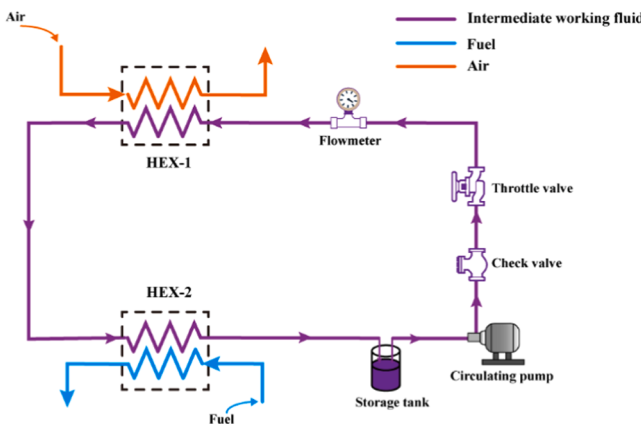


Fig. 1. The schematic of the intermediate heat-exchange cycle system for aero engines.

capacity and outlet conditions [18]. For the intermediate heat-exchange cycle, weight optimization is to some extent equivalent to the optimization of the heat transfer area for the fixed material. However, the existing research in this area mainly concentrates on the maximization of the Coefficient of Performance (COP), minimization of work input, maximization of heat transfer capacity, and minimization of entropy generation to reduce fuel consumption, research on total heat transfer area minimization is limited. For example, Bejan [19] examined the progress and implementation of entropy generation minimization across various sectors of mainstream thermal engineering and science, and pointed out that the approach to entropy generation minimization could uncover new opportunities for industrial research and development. Jing [20] developed a new approach using entransy transfer efficiency to determine the intermediate temperature relative to the maximum power for an endoreversible combined cycle plants within n-stage. With the aim of simultaneously optimizing the total heat transfer area, entropy generation, and power consumption, Yin et al. [21] utilized genetic algorithms to examine series-parallel and parallel heat recovery systems. A thermodynamic model to simulate a  $\text{SCO}_2$  cycle for waste heat recovery was constructed by Na et al. [22], and the allocation of HEXs with the fixed total  $UA$  value was optimized to achieve the maximum net power. Song et al. [23,24] investigated the optimal intermediate medium temperature in a combined transcritical  $\text{CO}_2$  and  $\text{R}134\text{a}$  heat pump for space heating, at which the combined system had the highest COP. As the temperature of the medium increased, the results revealed a decline in system power dissipation, along with an initial increase and subsequent decrease in heating capacity. Wang et al. [25] proposed a novel optimization method that utilizes the cascade of cold sources to reduce fuel consumption in the precooled engine cycle. Chen et al. [26] derived the analytical expressions for the optimal allocation of heat-exchanger areas for refrigeration and air-conditioning plants. The minimization of the total heat transfer area and heat conductance of heat pumps and irreversible refrigerators was analytically studied by Sarkar and Bhattacharyya [18] and verified the results through numerical simulation. Nevertheless, it should be emphasized that the aforementioned findings are deficient in their coverage of total heat transfer area minimization, particularly when it comes to aero engines, which are of significant importance in reducing the weight and space occupation and increase the thrust-to-weight ratio. Specifically, the current design practice lacks a theoretical foundation when it comes to selecting the parameters of the intermediate working fluid.

The objective of this study is to present a convenient method for determining the IWF mass flow rate and temperature within an intermediate heat-exchange cycle for aero engines corresponding to the minimization of the overall heat transfer area. Theoretical studies have been carried out considering three distinct conditions of the IWF mass flow rate and intermediate operating temperature, respectively. Finally,

the theoretical findings have been validated by comparing them with the results obtained through numerical computations. The current study offers significant flexibility to designers in determining the IWF mass flow rate and intermediate operating temperature.

## 2. System description

Fig. 1 depicts the working principle of the intermediate heat-exchange cycle for aero engines, including three working fluids: air, fuel, and IWF. Different fluids correspond to different heat sources based on the fluid temperature. Fuel, air, and IWF represent low-temperature heat sources, high-temperature heat sources, and medium-temperature heat sources, respectively. For the IWF flow path, IWF is stored in a storage tank and driven by the circulating pump that makes it circulate throughout the system. The throttle valve adjusts the IWF mass flow rate to the design point. At first, IWF flows through the HEX-1 to cool down the air. After absorbing the heat from the high-temperature heat sources, the IWF temperature rises. Hereupon, IWF flows through the HEX-2 to preheat the fuel and then flows back to the storage tank, finishing one cycle. Through the refined design of HEX-1 and HEX-2 and the regulation of IWF mass flow rate, the initial IWF temperature at each cycle is basically constant at the steady state, thus forming a closed cycle. For the air flow path, depending on the application requirements of the intermediate heat-exchange cycle system, air can come from the inlet ram air, compressor bleed air, or the bearing chamber cooling air. After cooling in the HEX-1, cooled air flows into the compressor or the turbine, which enhances the aero-engine performance. As for the fuel flow path, the high-temperature fuel is injected into the combustor after heat absorption in the HEX-2.

## 3. Mathematical model

The circulation parameters of IWF are crucial for designing an intermediate heat-exchange cycle system with well comprehensive performance, particularly the intermediate temperature and mass flow rate. The intermediate temperature is defined as the IWF inlet temperature of HEX-1. The design of HEX-1 and HEX-2 is influenced differently by the intermediate temperature. Under the constant constraints of temperature and mass flow rate for the fuel and air flow path, decreasing the intermediate temperature increases the temperature difference of HEX-1, thereby reducing the required heat transfer area. However, the intermediate temperature also has an impact on the design of HEX-2. The decrease in the IWF inlet temperature of HEX-2 is not conducive to preheating the fuel, which means the larger design heat transfer area of HEX-2. Hence, the low intermediate temperature enhances the performance of HEX-1 while inhibiting the performance of HEX-2. The trade-off between the HEX-1 and HEX-2 performances affects the performance of the intermediate heat-exchange cycle system, and there exists an optimal intermediate temperature. As to the IWF mass flow rate, there is the problem of optimal selection as well. As the IWF mass flow rate increases, it is beneficial for cooling the air and thereby reduces the design heat transfer area of HEX-1. Nevertheless, the IWF outlet temperature of HEX-1 simultaneously decreases, leading to an enlargement of the design heat transfer area of HEX-2. Although the increase in mass flow rate enhances heat transfer and leads to an improvement in the overall heat transfer coefficient, the primary factor in the design of HEXs remains the mean temperature difference of heat exchange at this point. In conclusion, the total heat transfer area of the intermediate heat-exchange cycle system depends on the trade-off between HEX-1 and HEX-2. This indicates that the optimal circulation parameters of IWF exist, including the IWF mass flow rate and intermediate temperature. At the optimal circulation parameters, the individual design heat transfer area of HEX-1 and HEX-2 may not have the minimum value. However, the intermediate heat-exchange cycle system provides the minimum design heat transfer area (i.t. the minimum system weight).

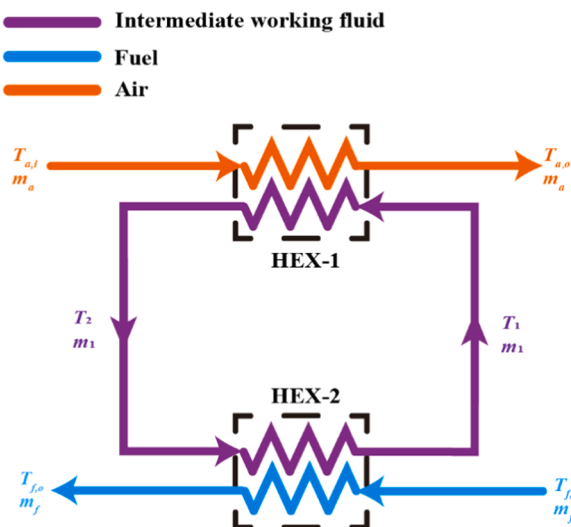


Fig. 2. The schematic of the intermediate heat-exchange cycle thermodynamic model.

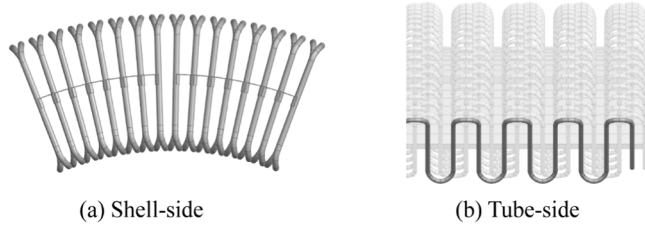


Fig. 3. Cross-sectional view of the heat exchanger.

Table 1  
Boundary conditions for the circulation parameters of IWF.

No.	Intermediate temperature	The mass flow rate of IWF
Case A	Uncertain	Certain
Case B	Certain	Uncertain
Case C	Uncertain	Uncertain

### 3.1. The intermediate cycle thermodynamic model

To study the effect of the circulation parameters on the intermediate heat-exchange cycle, a mathematical model is established as presented in Fig. 2. The intermediate heat-exchange cycle thermodynamic model contains the IWF mass flow rate  $m_1$ , the fuel mass flow rate  $m_f$ , the air mass flow rate  $m_a$ , the intermediate temperature  $T_1$ , the IWF outlet temperature of HEX-1 and the IWF inlet temperature of HEX-2  $T_2$ , the air inlet and outlet temperature  $T_{a,i}$  and  $T_{a,o}$ , the fuel inlet and outlet temperature  $T_{f,i}$  and  $T_{f,o}$ . To simplify the analysis for the theoretical derivation, the system model is on the basis of the assumptions below: 1) parameters of each state point are steady; 2) all the components are

both HEX-1 and HEX-2 are shell-and-tube HEXs with IWF flowing through the tubes. The cross-section of the shell side and tube side of the heat exchanger is illustrated in Fig. 3. Two serpentine tubes are parallelly placed in the same row, and several rows of tube bundles form the heat exchanger core; 6) HEX-1 and HEX-2 are counter-flow types. Considering the actual working conditions of the aero engine, there are three boundary conditions for the circulation parameters of IWF as illustrated in Table 1.

The heat transfer rate of each HEX  $Q_i$  can be calculated according to the energy balance equations:

$$Q_1 = m_a c_{p,a} (T_{a,i} - T_{a,o}) = m_1 c_{p,w} (T_2 - T_1) \quad (1)$$

$$Q_1 = m_a c_{p,a} (T_{a,i} - T_{a,o}) = U_{o,1} A_1 \Delta T_{m,1} \quad (2)$$

$$Q_2 = m_f c_{p,f} (T_{f,o} - T_{f,i}) = m_1 c_{p,w} (T_2 - T_1) \quad (3)$$

$$Q_2 = m_f c_{p,f} (T_{f,o} - T_{f,i}) = U_{o,2} A_2 \Delta T_{m,2} \quad (4)$$

where  $U_{o,i}$  is the overall heat transfer coefficient of HEX based on the heat transfer area in the tube,  $A_i$  is the heat transfer area in the tube of each HEX,  $c_{p,a}$   $c_{p,w}$   $c_{p,f}$  is the isobaric specific heat capacity of air, IWF, and fuel, respectively,  $\Delta T_{m,i}$  is the mean temperature difference, generally, it can be expressed as follows:

$$\Delta T_{m,1} = \frac{(T_{a,i} - T_2) - (T_{a,o} - T_1)}{\ln[(T_{a,i} - T_2)/(T_{a,o} - T_1)]} \quad (5)$$

$$\Delta T_{m,2} = \frac{(T_2 - T_{f,o}) - (T_1 - T_{f,i})}{\ln[(T_2 - T_{f,o})/(T_1 - T_{f,i})]} \quad (6)$$

Combining Eq. (1)–(6) gives the heat transfer area of HEX-1 and HEX-2, and the function of  $T_2$  with respect to  $T_1$ , which are

$$A_1 = \frac{m_a c_{p,a}}{\left(1 - \frac{m_a c_{p,a}}{m_1 c_{p,w}}\right) U_{o,1}} \ln \frac{T_{a,i} - T_1 - Q_1 / (m_1 c_{p,w})}{T_{a,o} - T_1} \quad (7)$$

$$A_2 = \frac{m_f c_{p,f}}{\left(\frac{m_f c_{p,f}}{m_1 c_{p,w}} - 1\right) U_{o,2}} \ln \frac{T_1 - T_{f,o} + Q_2 / (m_1 c_{p,w})}{T_1 - T_{f,i}} \quad (8)$$

$$T_2 = \frac{m_a c_{p,a}}{m_1 c_{p,w}} (T_{a,i} - T_{a,o}) + T_1 = \frac{m_f c_{p,f}}{m_1 c_{p,w}} (T_{f,o} - T_{f,i}) + T_1 \quad (9)$$

The determination of the intermediate heat-exchange cycle's total heat transfer area ( $A_{total}$ ) can be achieved through the utilization of Eq. (10). As evidenced by this equation,  $A_{total}$  is primarily impacted by several key factors, including the thermal properties of working fluids, the intermediate temperature ( $T_1$ ), the IWF mass flow rate ( $m_1$ ), and the overall heat transfer coefficient of each HEX ( $U_{o,i}$ ). During the design phase of the intermediate heat-exchange cycle system scheme, the thermal management scheme employed in aero engines may impose limitations on the IWF mass flow rate and temperature. As such, it is imperative to conduct a separate analysis for different constraint scenarios of IWF.

$$A_{total}(T_1) = A_1 + A_2 = \frac{m_a c_{p,a}}{\left(1 - \frac{m_a c_{p,a}}{m_1 c_{p,w}}\right) U_{o,1}} \ln \frac{T_{a,i} - T_1 - Q_1 / (m_1 c_{p,w})}{T_{a,o} - T_1} + \frac{m_f c_{p,f}}{\left(\frac{m_f c_{p,f}}{m_1 c_{p,w}} - 1\right) U_{o,2}} \ln \frac{T_1 - T_{f,o} + Q_2 / (m_1 c_{p,w})}{T_1 - T_{f,i}} \quad (10)$$

adiabatic except for HEXs; 3) the thermal properties of working fluids are constant; 4) all boundary conditions for air and fuel are constant; 5)

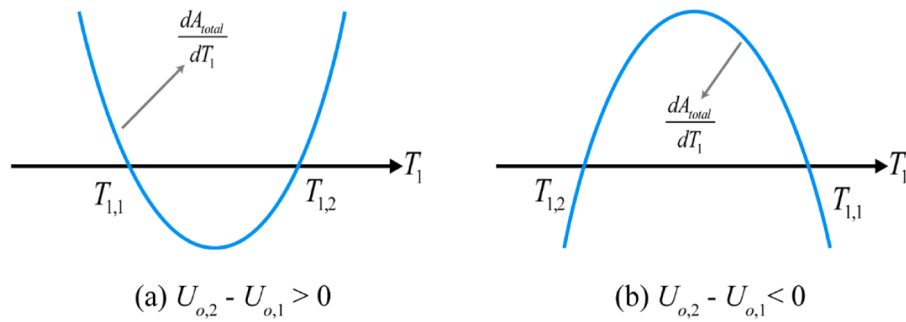


Fig. 4. The variation trend of  $\frac{dA_{total}}{dT_1}$  with  $T_1$ .

### 3.2. Case A - fixed IWF mass flow rate

For a fixed IWF mass flow rate, given the assumption of constant thermal properties for the working fluids and the HEX structure is certain,  $U_{o,i}$  can be regarded as a constant value. What's more, under the assumption that all the components are adiabatic except for HEXs, the heat transfer rate of two HEX is equal as shown in Eq. (11). Therefore, Eq. (10) becomes a univariate function of  $A_{total}$  with respect to  $T_1$ . To uncover the variation trend in  $A_{total}$  with the intermediate temperature  $T_1$ , the derivative of Eq. (10) to  $T_1$  can be represented in Eq. (12).

$$Q_{equal} = Q_1 = Q_2 \quad (11)$$

$$\frac{dA_{total}}{dT_1} = Q_{equal} \frac{\left[ U_{o,1}(T_{a,i} - T_2) + U_{o,2}(T_2 - T_{f,o}) \right] T_1}{U_{o,1} U_{o,2} (T_{a,o} - T_2) (T_{a,o} - T_1) (T_2 - T_{f,o}) (T_1 - T_{f,i})} - Q_{equal} \frac{U_{o,1} T_{a,o} (T_{a,i} - T_2) + U_{o,2} T_{f,i} (T_2 - T_{f,o})}{U_{o,1} U_{o,2} (T_{a,o} - T_2) (T_{a,o} - T_1) (T_2 - T_{f,o}) (T_1 - T_{f,i})} \quad (12)$$

Where  $Q_{equal}$  is the equilibrium heat transfer rate when the system is stable.

Notably, both  $Q_{equal}$  and the denominator of Eq. (12) maintain values greater than zero. This observation signifies that the positive or negative nature of the numerator of Eq. (12) can serve as an indicator of the trend of  $A_{total}$  variation. When set  $R_1 = \frac{m_1 c_{p,w}}{m_o c_{p,a}}$  and  $R_2 = \frac{m_1 c_{p,w}}{m_f c_{p,f}}$ , the numerator of Eq. (12) can be rewritten as:

$$\text{Numerator} = (U_{o,2} - U_{o,1}) T_1^2 + \left[ \frac{U_{o,2}}{R_2} (T_{f,o} - T_{f,i}) - \frac{U_{o,1}}{R_1} (T_{a,i} - T_{a,o}) - U_{o,2} (T_{f,o} + T_{f,i}) + U_{o,1} (T_{a,i} + T_{a,o}) \right] T_1 - \frac{U_{o,2} T_{f,i} (T_{f,o} - T_{f,i}) + U_{o,1} T_{a,o} (T_{a,i} - T_{a,o}) + U_{o,2} T_{f,i} T_{f,o} - U_{o,1} T_{a,i} T_{a,o}}{R_2} \quad (13)$$

Equating Eq. (13) to zero, when set, the extreme value point is obtained with the following expressions:

$$T_{1,1} = \frac{\frac{T_{a,i} - T_{a,o}}{R_1} (U_{o,1} - U_{o,2}) - U_{o,1} (T_{a,i} + T_{a,o}) + U_{o,2} (T_{f,i} + T_{f,o})}{2(U_{o,2} - U_{o,1})} - \frac{\frac{T_{a,i} - T_{a,o}}{R_1} \sqrt{[(R_1 - 1)U_{o,1} - (R_2 - 1)U_{o,2}]^2 + 2U_{o,1}U_{o,2}(1 - \sigma)R_1R_2}}{2R_1(U_{o,2} - U_{o,1})} \quad (14)$$

$$T_{1,2} = \frac{\frac{T_{a,i} - T_{a,o}}{R_1} (U_{o,1} - U_{o,2}) - U_{o,1} (T_{a,i} + T_{a,o}) + U_{o,2} (T_{f,i} + T_{f,o})}{2(U_{o,2} - U_{o,1})} + \frac{\frac{T_{a,i} - T_{a,o}}{R_1} \sqrt{[(R_1 - 1)U_{o,1} - (R_2 - 1)U_{o,2}]^2 + 2U_{o,1}U_{o,2}(1 - \sigma)R_1R_2}}{2R_1(U_{o,2} - U_{o,1})} \quad (15)$$

where set  $\sigma = \frac{(T_{f,i} + T_{f,o})(T_{a,i} + T_{a,o}) - 2T_{f,i}T_{f,o} - 2T_{a,i}T_{a,o}}{(T_{a,i} - T_{a,o})(T_{f,o} - T_{f,i})}$ .

In consideration of the sign of  $U_{o,2} - U_{o,1}$ , two distinct trends regarding the variation of Eq. (12) emerge. In Fig. (4), when  $U_{o,2} - U_{o,1} > 0$ ,  $A_{total}$  displays a non-monotonic behavior with increasing  $T_1$ : initially decreasing, then increasing, and finally decreasing again. Conversely, when  $U_{o,2} - U_{o,1} < 0$ ,  $A_{total}$  exhibits the opposite trend. Notably, the local minimum point of Eq. (10) occurs at  $T_{1,2}$  for both scenarios. Consequently, for a fixed IWF mass flow rate within the range of  $T_1 \in [T_{1,1}, T_{1,2}]$ , the optimal  $T_1$  that minimizes  $A_{total}$  can be determined through the expression below:

$$T_{1,optimal} = \min \{A_{total}|_{T_{1,2}}, A_{total}|_{T_{1,1}}, A_{total}|_{T_{1,right}}\} \quad (16)$$

### 3.3. Case B - fixed intermediate temperature

For a fixed intermediate temperature, when calculating the optimal IWF mass flow rate,  $U_{o,i}$  cannot be considered constant since  $U_{o,i}$  will

change with the Reynolds number ( $Re$ ). It can be expressed as Eq. (17).

$$U_{o,i} = \frac{1}{\frac{1}{h_i} + \frac{d_i}{2k_0} \ln \frac{d_o}{d_i} + \frac{1}{h_o} \frac{d_i}{d_o}} \quad (17)$$

where  $h_o$  is the heat transfer coefficient of the shell side,  $h_i$  is the heat transfer coefficient of the tube side,  $d_b$ ,  $d_o$ , and  $k_0$  represent the tube's inner diameter, tube's outer diameter, and thermal conductivity of the tube wall, respectively. Due to the given geometry and the certain boundary conditions for the shell-side working fluid,  $h_o$  remains constant for each HEX [21]. As for the heat transfer of IWF in the tube flow, the Nusselt number ( $Nu$ ) correlation can be considered in the form of the Dittus-Boelter formula as

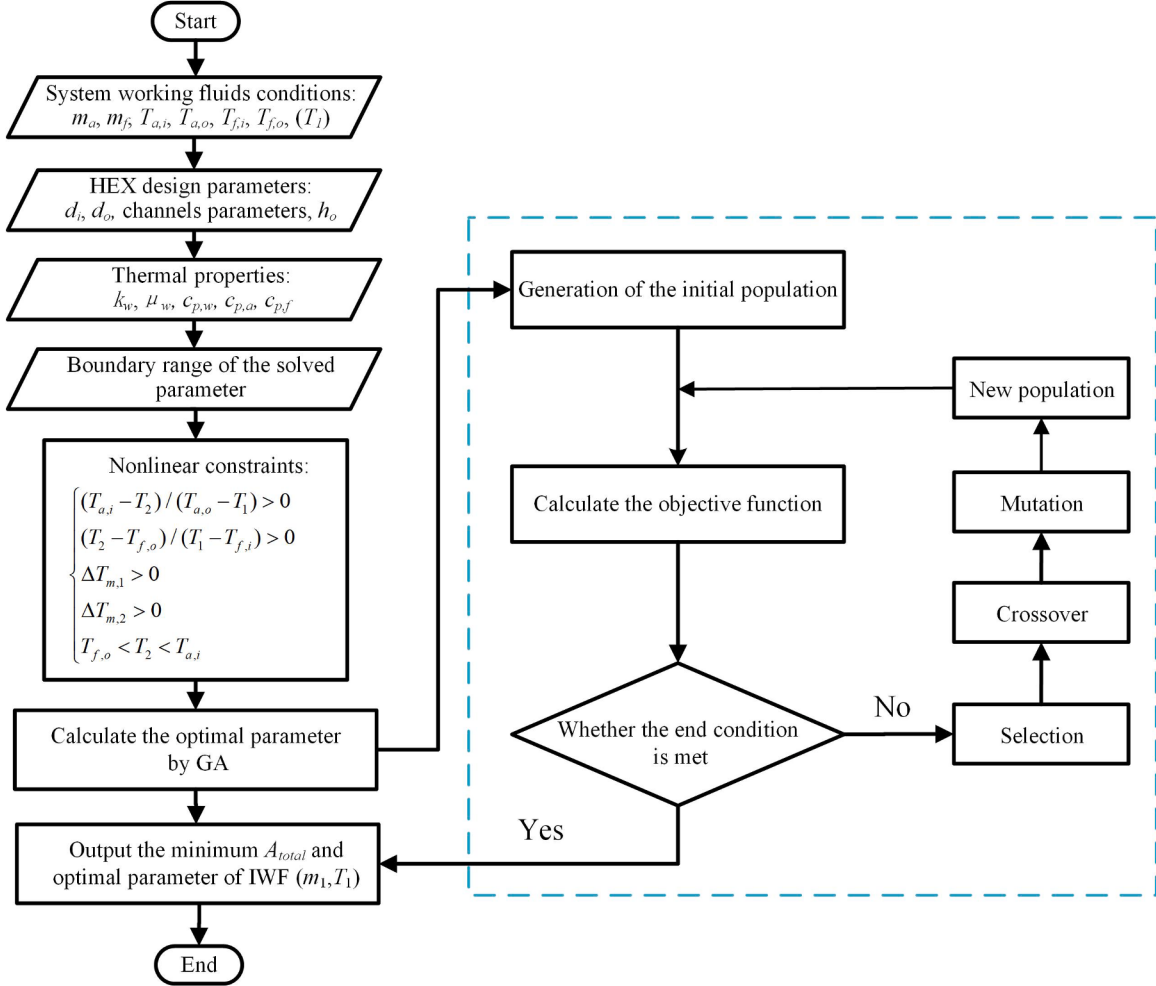


Fig. 5. The flowchart of optimal parameter calculation with GA optimization.

Table 2  
Optimum design conditions for a fixed IWF mass flow rate.

Parameters	Values	Parameters	Values
$m_a$ (kg/s)	0.73	$T_{a,i}$ (°C)	543
$m_f$ (kg/s)	1.03	$T_{a,o}$ (°C)	342
$m_1$ (kg/s)	0.46	$T_{f,i}$ (°C)	150
$c_{p,a}$ (J/kg/K)	1079.7	$T_{f,o}$ (°C)	210.8
$c_{p,f}$ (J/kg/K)	2529.1	$P_{a,i}$ (MPa)	0.55
$c_{p,w}$ (J/kg/K)	4839.4	$P_{f,i}$ (MPa)	6.28
$U_{o,1}$ (W/m <sup>2</sup> /K)	900	$P_1$ (MPa)	10
$U_{o,2}$ (W/m <sup>2</sup> /K)	5100		

$$Nu_i = C_1 Re_w^a Pr_w^b = \frac{h_i d_i}{k_w} \quad (18)$$

where  $C_1$ ,  $a$ , and  $b$  are the undetermined coefficients,  $Re_w$ ,  $Pr_w$ , and  $k_w$  represent the Reynolds number, Prandtl number, and thermal conductivity of IWF, respectively.  $Re_w$  is defined as

$$Re_w = \frac{4m_1}{\mu_w \pi d_i} \quad (19)$$

where  $\mu_w$  is the dynamic viscosity of IWF.

When set  $\alpha = \left(\frac{4}{\mu_w \pi}\right)^a C_1 k_w Pr_w^b$  and  $\beta = \frac{d_i}{2k_0} \ln \frac{d_o}{d_i} + \frac{1}{h_o} \frac{d_i}{d_o}$ , combining Eq. (18) and Eq. (19) gives the heat transfer coefficient of IWF flowing in the

tube,  $U_{o,1}$ , and  $U_{o,2}$  as follows

$$h_i = \alpha m_1^a \quad (20)$$

$$U_{o,1} = \frac{\alpha_1 m_1^a}{1 + \alpha_1 \beta_1 m_1^a} \quad (21)$$

$$U_{o,2} = \frac{\alpha_2 m_1^a}{1 + \alpha_2 \beta_2 m_1^a} \quad (22)$$

Combining Eq. (2) (4) (11) (21) and (22), the following expression is obtained for  $A_{total}$  for a fixed intermediate temperature:

$$A_{total}(m_1) = Q_{equal} \left( \frac{1 + \alpha_1 \beta_1 m_1^a}{\alpha_1 m_1^a \Delta T_{m,1}} + \frac{1 + \alpha_2 \beta_2 m_1^a}{\alpha_2 m_1^a \Delta T_{m,2}} \right) \quad (23)$$

The logarithmic mean temperature difference (LMTD) consistently serves as the maximum heat transfer driving force when two fluids flow in opposite directions [27]. Nevertheless, when the heat capacities of two fluids are equal, LMTD is no longer applicable. For this situation, the arithmetic mean temperature difference (AMTD) is adopted instead of LMTD. It is easy to demonstrate that when  $\Delta T_{max} / \Delta T_{min} < 1.2$  holds, the difference between LMTD and AMTD is less than 0.277%. Consequently, to calculate the total heat transfer area for a fixed intermediate temperature, the mean temperature difference in Eq. (23) is expressed as

$$\left\{ \begin{array}{l} \text{when } \frac{\max\{(T_{a,i} - T_2), (T_{a,o} - T_1)\}}{\min\{(T_2 - T_{f,o}), (T_{a,o} - T_1)\}} \leq 1.2, \quad \left\{ \begin{array}{l} \Delta T_{m,1} = \frac{T_{a,i} - T_2 + T_{a,o} - T_1}{2} \\ \Delta T_{m,2} = \frac{T_2 - T_{f,o} + T_1 - T_{f,i}}{2} \end{array} \right. \\ \text{when } \frac{\max\{(T_{a,i} - T_2), (T_{a,o} - T_1)\}}{\min\{(T_2 - T_{f,o}), (T_{a,o} - T_1)\}} > 1.2, \quad \left\{ \begin{array}{l} \Delta T_{m,1} = \frac{(T_{a,i} - T_2) - (T_{a,o} - T_1)}{\ln[(T_{a,i} - T_2)/(T_{a,o} - T_1)]} \\ \Delta T_{m,2} = \frac{(T_2 - T_{f,o}) - (T_1 - T_{f,i})}{\ln[(T_2 - T_{f,o})/(T_1 - T_{f,i})]} \end{array} \right. \end{array} \right. \quad (24)$$

By combining Eqs. (23) and (24), a transcendental equation can be obtained as a univariate function of  $A_{total}$  with respect to  $m_1$ . However, the derivative of this equation to  $m_1$  will be a transcendental equation and cannot be solved directly for the extreme value point to obtain the optimal IWF mass flow rate as in Section 3.2. Therefore, the genetic algorithm (GA) is employed to calculate the optimal  $m_1$  in Section 3.5.

#### 3.4. Case C - $T_1$ and $m_1$ are variable

Under the condition of both the  $T_1$  and  $m_1$  variable, it requires the use of an optimization algorithm to calculate the optimal parameters to minimize  $A_{total}$ . Consistent with the approach in Section 3.3, the expression of the objective function can be obtained as Eq. (24) and (25). The only difference with Eq. (23) is that it has two variables  $T_1$  and  $m_1$ . In Section 3.5, the problem is addressed using the genetic algorithm.

$$A_{total}(m_1, T_1) = Q_{equal} \left( \frac{1 + \alpha_1 \beta_1 m_1^a}{a_1 m_1^a \Delta T_{m,1}} + \frac{1 + \alpha_2 \beta_2 m_1^a}{a_2 m_2^a \Delta T_{m,2}} \right) \quad (25)$$

#### 3.5. Genetic algorithm for optimal parameters of IWF

For the situation in Section 3.3 and Section 3.4, the optimal parameters of IWF that minimize the  $A_{total}$  are sought using the GA. GA, leveraging the pattern theorem and the building block hypothesis, demonstrates its efficacy as a powerful global search method [28,29]. To avoid obtaining suboptimal solutions, appropriate methods such as mating, recombination, and replacement strategies are employed by GA [30]. Consequently, the optimization processes in GA make use of the reproduction, crossover, and mutation operators. GA has been successfully used in HEX designs [31–33].

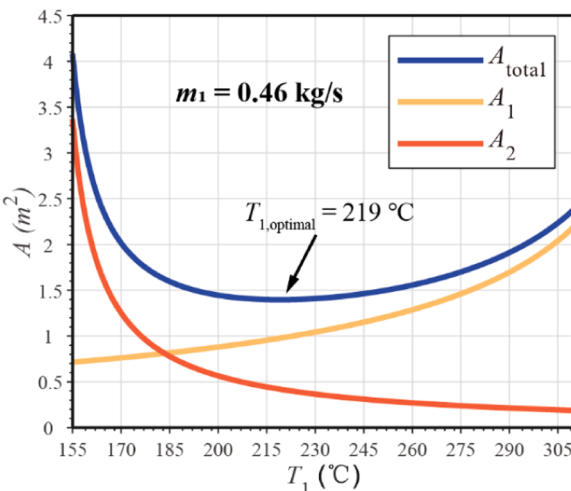


Fig. 6. Heat transfer area of HEXs varies with  $T_1$  for a fixed IWF mass flow rate.

The calculation procedure of the optimal parameters with GA optimization is given in Fig. 5. The only difference between the calculation process of the two cases in Sections 3.3 and 3.4 is whether  $T_1$  is given, and Section 3.3 corresponds to the case where  $T_1$  is known. As mentioned, the determination of the optimal parameter relies on a series of pre-selected parameters, including the system working fluids conditions, HEX design parameters, thermal properties, and so on. GA searches for optimal results with the objective function to evaluate the  $A_{total}$ . In the current study, the objective function is shown as Eq. (23) and Eq. (25), respectively. To obtain the appropriate results meeting the first law of thermodynamics, nonlinear constraints should be added to the calculation process of the GA. Since IWF is a cold source in HEX-1 and a heat source in HEX-2, there is  $T_{f,o} < T_2 < T_{a,i}$ . Moreover, it should be ensured that  $\Delta T_m$  is greater than zero to make the heat transfer rate greater than zero. For the purpose of avoiding imaginary numbers in logarithmic calculations, the interior of the logarithmic term should be positive. Considering the aforementioned conditions, the nonlinear constraints are listed as Eq. (26). When the end condition is met, the minimum  $A_{total}$  and optimal parameters of IWF will be output. With the output parameters, the minimum  $A_{total}$  for the intermediate heat-exchange cycle system is expected to be obtained, resulting in a minimum system weight. The lightweight of the intermediate heat-exchange cycle system is valued most according to the aircraft demand.

$$\left\{ \begin{array}{l} \frac{(T_{a,i} - T_2)}{(T_{a,o} - T_1)} > 0 \\ \frac{(T_2 - T_{f,o})}{(T_1 - T_{f,i})} > 0 \\ \Delta T_{m,1} > 0 \\ \Delta T_{m,2} > 0 \\ T_{f,o} < T_2 < T_{a,i} \end{array} \right. \quad (26)$$

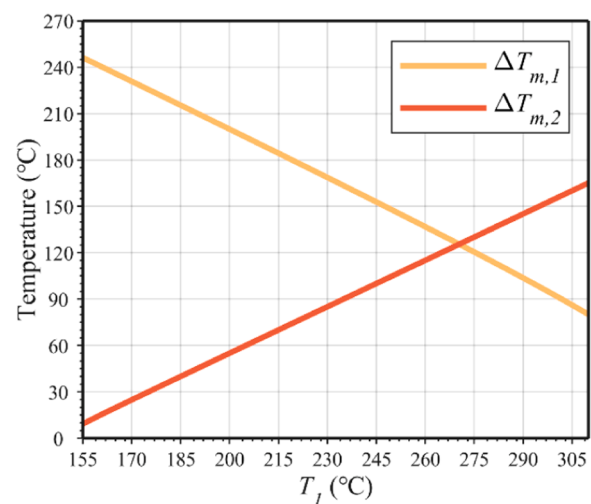


Fig. 7. Mean temperature difference of each HEX varies with  $T_1$  in the case of  $m_1 = 0.46 \text{ kg/s}$ .

**Table 3**Optimal calculation results for the given  $m_1$ .

$m_1$ (kg/s)	$T_{1,optimal}$ (°C)	$A_{total}$ (m <sup>2</sup> )
0.2	187.5	1.419
0.3	204.5	1.389
0.4	214.5	1.392
0.5	221.5	1.401

The problem of determining the optimal parameters will be addressed using the GA toolbox in Matlab R2021b [34]. The GA toolbox has been configured with default parameter settings, with the exception of the stopping criteria, which has been specifically set to include a maximum generation of 150, a constraint tolerance of  $10^{-20}$ , and a function tolerance of  $10^{-50}$ .

#### 4. Case study and discussion

In this study, an intermediate heat-exchange cycle system for aero engines, as illustrated in Fig. 1, is evaluated with Chinese aviation kerosene RP-3 as the fuel. The water is chosen as the IWF as it is a common cooling medium, and the existing anti-icing measures for water in the low-temperature environment of aircraft engines are relatively mature. Boiling water can have a bad effect on the stability and reliability of the system. Since boiling water is often accompanied by the formation of bubbles and turbulence, which can affect the hydraulic

characteristics within the system. This may result in shocks and vibrations to components such as pipelines and valves, which is not conducive to the stable operation of the intermediate heat-exchange cycle system.

**Table 4**

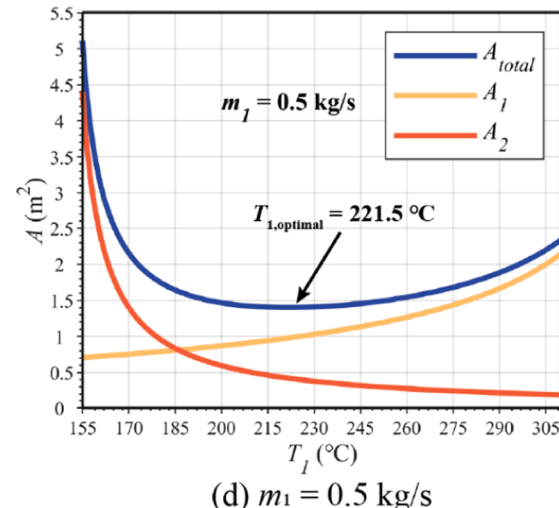
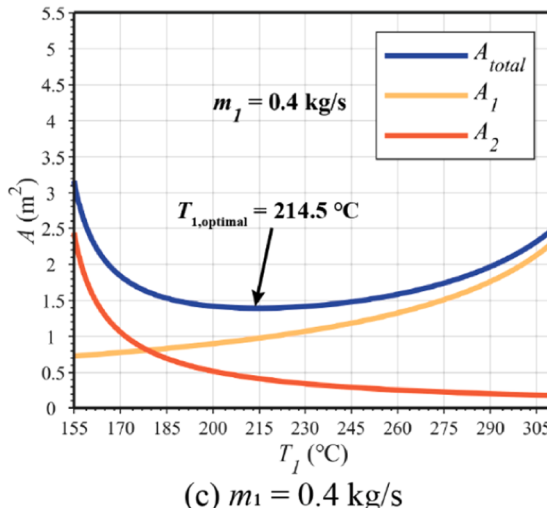
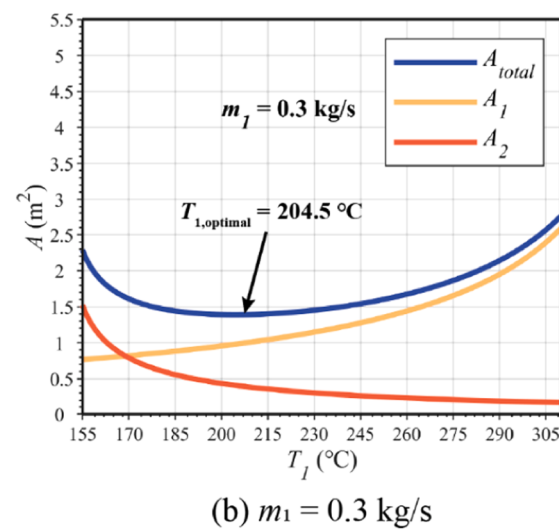
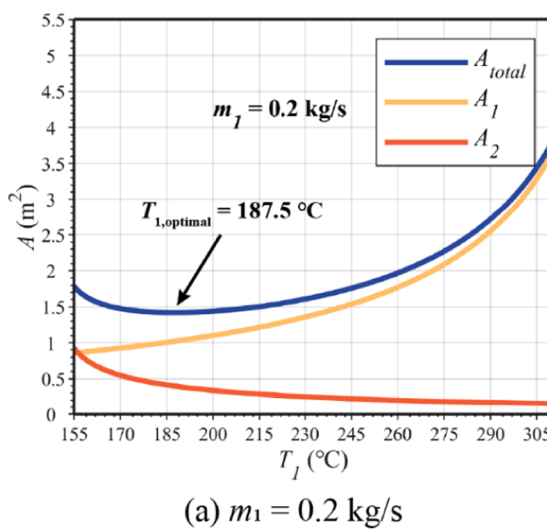
Optimum design conditions for a fixed intermediate temperature.

Parameters	Values	Parameters	Values
$T_1$ (°C)	180	$T_{a,i}$ (°C)	543
$m_f$ (kg/s)	1.03	$T_{a,o}$ (°C)	342
$m_a$ (kg/s)	0.73	$T_{f,i}$ (°C)	150
$c_{p,a}$ (J/kg/K)	1079.7	$T_{f,o}$ (°C)	210.8
$c_{p,f}$ (J/kg/K)	2529.1	$P_{a,i}$ (MPa)	0.55
$c_{p,w}$ (J/kg/K)	4839.4	$P_{f,i}$ (MPa)	6.28
$h_{o,1}$ (W/m <sup>2</sup> /K)	750	$P_1$ (MPa)	10
$h_{o,2}$ (W/m <sup>2</sup> /K)	8000		

**Table 5**

Structure parameters of each HEX.

	HEX-1	HEX-2
Material	316L Stainless Steel	316L Stainless Steel
$\lambda_0$ (W/m/K)	16.2	16.2
$d_i$ (mm)	1.4	1.2
$d_o$ (mm)	1.8	1.6
$N_{tube}$	96	96

**Fig. 8.** Heat transfer area of HEXs varies with  $T_I$  for different fixed IWF mass flow rates.

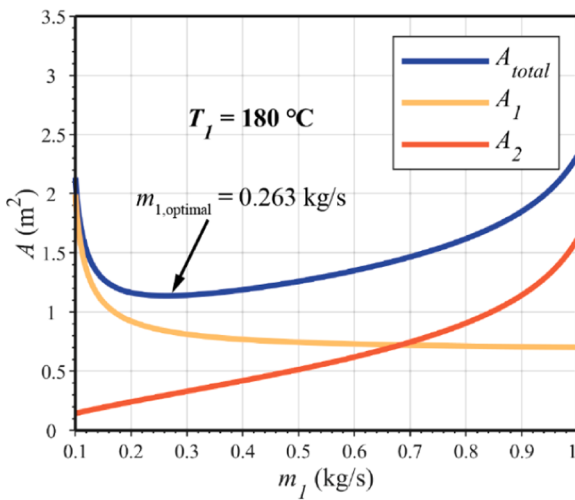


Fig. 9. Heat transfer area of HEXs varies with  $m_1$  for a fixed intermediate temperature.

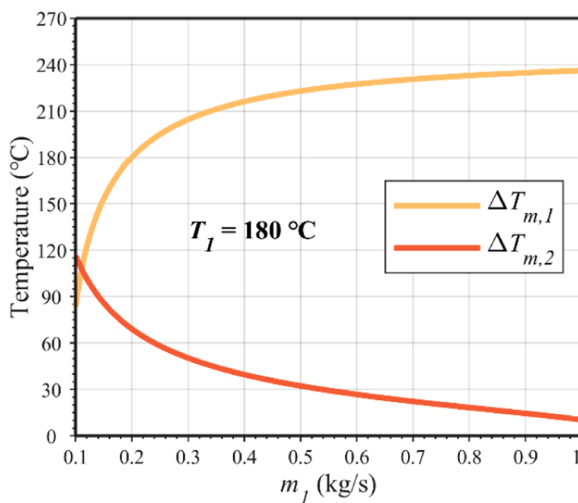


Fig. 10. Mean temperature difference of each HEX varies with  $m_1$  in the case of  $T_1 = 180^\circ\text{C}$ .

Table 6

Optimal calculation results for the given  $T_1$ .

$T_1$ (°C)	$m_{1,optimal}$ (kg/s)	$A_{total}$ (m <sup>2</sup> )
180	0.263	1.138
200	0.374	1.126
220	0.613	1.142
230	0.827	1.159

Furthermore, the boiling process introduces a gas phase. However the system is a closed-loop, if too much gas accumulates within the system, it may lead to increased pressure, which is not favorable for the safe operation of the system. Therefore, the water-side pressure is set at 10MPa, chosen due to the high boiling point of water ( $311^\circ\text{C}$ ) at this pressure, and IWF would be a single-phase working fluid. The physical properties of water and air are obtained from the package of CoolProp [35], while the physical properties of RP-3 are referred to [36–39]. Assuming both HEX-1 and HEX-2 are shell-and-tube HEXs referring [31, 40]. Based on the aforementioned investigation, the optimization calculation and analysis for the intermediate heat-exchange cycle are conducted for the specific case, and the accuracy of the algorithm is verified.

#### 4.1. Results of Case A - fixed IWF mass flow rate

To minimize the  $A_{total}$  for a fixed IWF mass flow rate, the optimum design condition is obtained from a case calculation of an intermediate heat-exchange cycle system for aero engines as illustrated in Table 2. Based on the boundary conditions of three working fluids and combined with the actual performance of the HEXs, set  $U_{o,1} = 900 \text{ W/m}^2\text{/K}$ ,  $U_{o,2} = 5100 \text{ W/m}^2\text{/K}$ , and  $T_1 \in [155^\circ\text{C}, 310^\circ\text{C}]$ .

Utilizing Eq. (15) and (16), the optimal value of  $T_1$  is determined to be  $219.07^\circ\text{C}$  and the minimum  $A_{total}$  is calculated to be  $1.397 \text{ m}^2$ . To validate the precision of the results, the current research employs Matlab R2021b to execute an iterative calculation for Eq. (7) and (8).  $T_1$  initiates at  $155^\circ\text{C}$  and is gradually increased by  $0.5^\circ\text{C}$  for each iteration until it reaches  $310^\circ\text{C}$ . Subsequently, the corresponding heat transfer area of each HEX is calculated. Through a traversal calculation process, the minimum value of  $A_{total}$  has been determined to be  $1.397 \text{ m}^2$ , which occurs at an optimal  $T_1$  value of  $219^\circ\text{C}$ . It deserves attention that a small error of 0.03% was encountered due to the relatively large increment of  $T_1$  utilized in the calculation. Nevertheless, it is anticipated that by using a smaller increment value for  $T_1$ , the traversal calculation results will align with the results obtained via Eq. (15) and (16). This confirms the accuracy of the theoretical formula, as presented in Eq. (15) and (16).

In Fig. 6, the heat transfer area of HEXs is illustrated as a function of

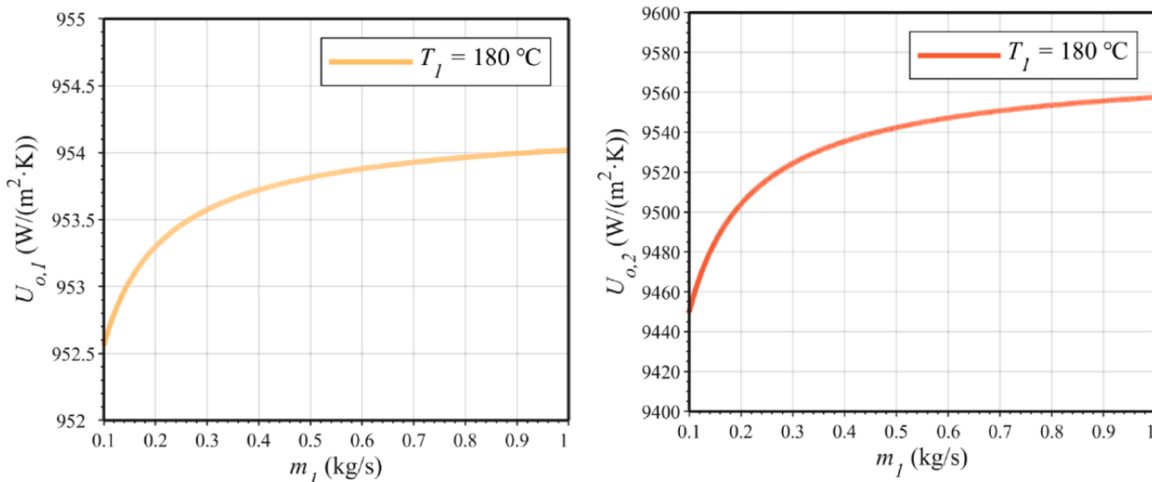


Fig. 11. Overall heat transfer coefficient of each HEX varies with  $m_1$  in the case of  $T_1 = 180^\circ\text{C}$ .

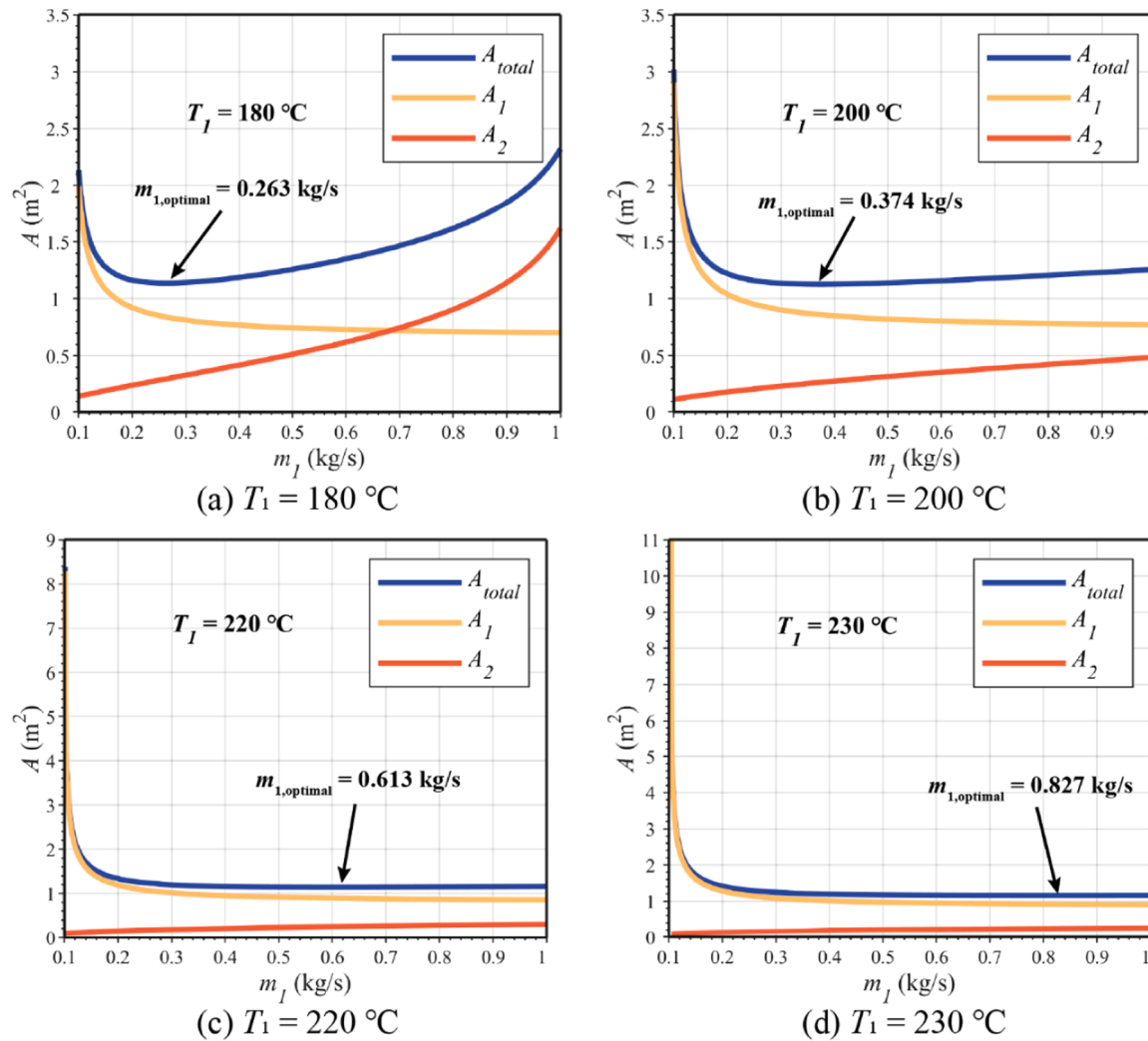


Fig. 12. Heat transfer area of HEXs varies with  $m_1$  for different fixed intermediate temperature.

$T_1$  for the specified  $m_1 = 0.46 \text{ kg/s}$ . As  $T_1$  increases,  $A_1$  exhibits a monotonic increase, whereas  $A_2$  demonstrates a monotonic decrease. The combined effect of  $A_1$  and  $A_2$  results in a non-monotonic variation of  $A_{total}$  as a function of  $T_1$ , initially decreasing before increasing. It also indicates the existence of an optimal  $T_1$  value, at which  $A_{total}$  reaches a minimum, leading to the system's lightest weight. Fig. 7 demonstrates the variations of the mean temperature difference of each HEX with  $T_1$  in the case of  $m_1 = 0.46 \text{ kg/s}$ . Since  $U_{o,i}$  and  $Q_i$  of each HEX are constant, for HEX-1, as  $T_1$  increases, it is not conducive to cooling air. And  $\Delta T_{m,1}$  exhibits a monotonic increase with the increment of  $T_1$ , resulting in monotonically increasing  $A_1$  according to Eq. (2). As for HEX-2, the elevated  $T_1$  is good for preheating the fuel, thus showing the opposite effect.

To study the effect of a given IWF mass flow rate on the optimal  $T_1$ , the present study calculates the optimal  $T_1$  and its corresponding  $A_{total}$  for four different given  $m_1$  using the above method. Table 3 shows the optimal calculation results for  $m_1 \in [0.2, 0.5] \text{ kg/s}$ , and Fig. 8 displays the variation of the heat transfer area of HEXs as a function of  $T_1$  for four different  $m_1$ . It should be noted that as the given  $m_1$  increases,  $T_{1,optimal}$  also increases. This is because when  $m_1$  is larger, it facilitates the IWF to cool the air at HEX-1, so  $T_2$  becomes smaller, i.e., the inlet temperature of the heat source at HEX-2 decreases. Considering the limiting situation, when  $T_2$  tends to  $T_{j,o}$ , the  $\Delta T_{m,2}$  becomes extremely small, resulting in  $A_2$  becoming large, which makes  $A_{total}$  large. Therefore, for larger  $m_1$  values, the optimal  $T_1$  would be higher to achieve better system

performance. However, there is no significant relationship between the value of the minimum  $A_{total}$  and the given  $m_1$ .

#### 4.2. Results of Case B - fixed intermediate temperature

The working conditions and structure parameters of each HEX to minimize the  $A_{total}$  for a fixed  $T_1$  are depicted in Table 4 and Table 5, respectively. By incorporating the performance of the HEXs with the boundary conditions of the three working fluids, set  $h_{o,1} = 750 \text{ W/m}^2/\text{K}$ ,  $h_{o,2} = 8000 \text{ W/m}^2/\text{K}$ , and  $m_1 \in [0.1 \text{ kg/s}, 1 \text{ kg/s}]$ .

The optimal value of  $m_1$  is determined to be  $0.263 \text{ kg/s}$ , and the minimum  $A_{total}$  is calculated to be  $1.138 \text{ m}^2$  using the algorithm mentioned in Section 3.5. During the calculation process, the calculation of the inner tube heat transfer coefficient  $h_i$  is conducted using the Dittus-Boelter correlation, as shown in Eq. (27) [41]. To validate the accuracy of the algorithm's computational results, a traversal calculation is carried out on the objective function Eq. (23). Specifically,  $m_1$  is divided into 10,000 equal intervals within its range, and the corresponding  $A_{total}$  values are calculated at each of these intervals. This process enables the determination of the minimum value of  $A_{total}$  and its corresponding value of  $m_1$ . Through the traversal calculation process, the minimum value of  $A_{total}$  has been determined to be  $1.138 \text{ m}^2$ , which occurs at an optimal  $m_1$  value of  $0.263 \text{ kg/s}$ . The same result confirms the accuracy of the proposed algorithm.

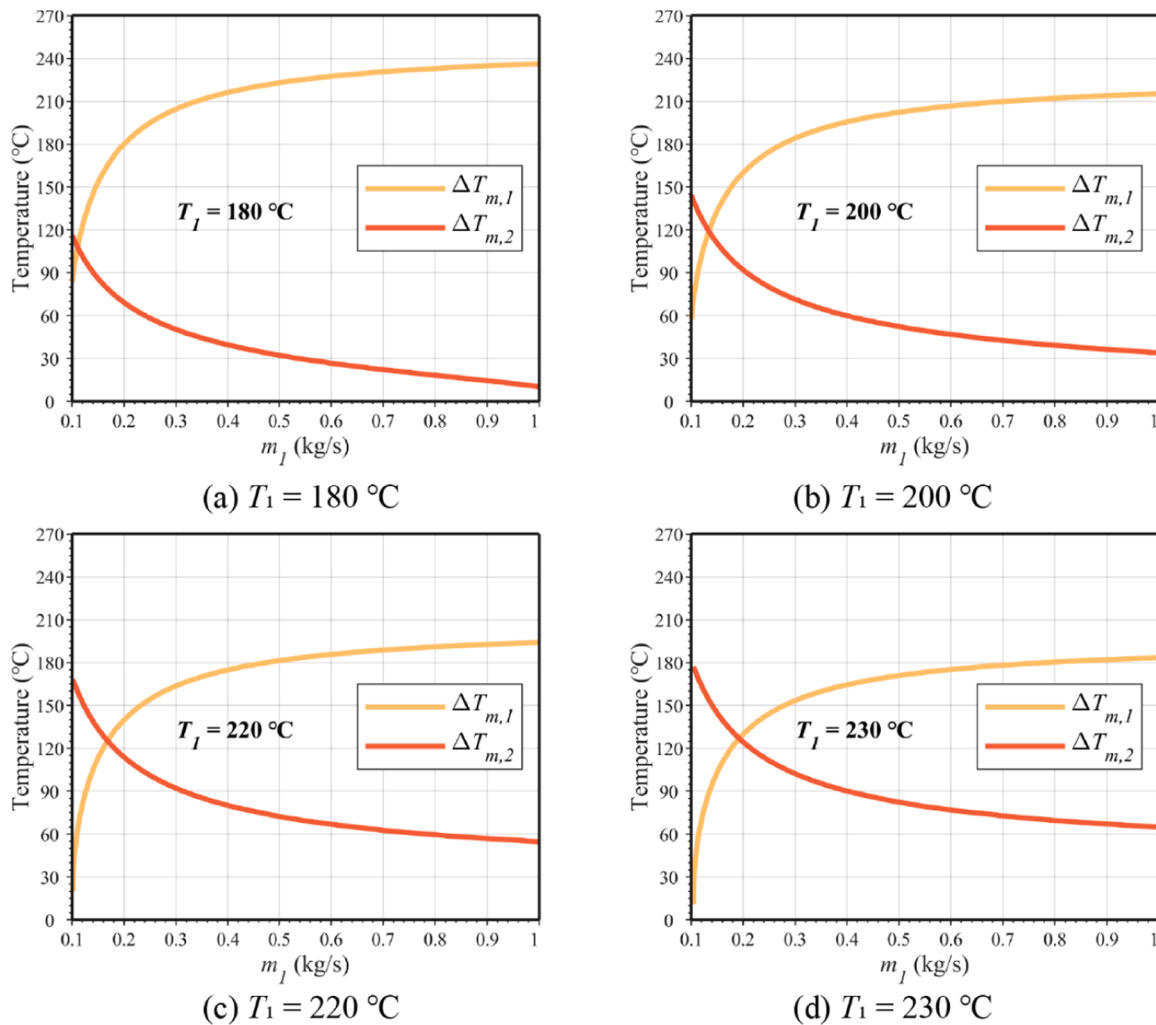


Fig. 13. Mean temperature difference of each HEX varies with  $m_1$  for different fixed intermediate temperature.

**Table 7**  
Optimum design conditions when both  $T_1$  and  $m_1$  variable.

Parameters	Values	Parameters	Values
$m_f$ (kg/s)	1.03	$T_{a,i}$ (°C)	543
$m_a$ (kg/s)	0.73	$T_{a,o}$ (°C)	342
$c_{p,a}$ (J/kg/K)	1079.7	$T_{f,i}$ (°C)	150
$c_{p,f}$ (J/kg/K)	2529.1	$T_{f,o}$ (°C)	210.8
$c_{p,w}$ (J/kg/K)	4839.4	$P_{a,i}$ (MPa)	0.55
$h_{o,1}$ (W/m <sup>2</sup> /K)	750	$P_{f,i}$ (MPa)	6.28
$h_{o,2}$ (W/m <sup>2</sup> /K)	8000	$P_1$ (MPa)	10

**Table 8**  
Optimal calculation results when both  $T_1$  and  $m_1$  variable.

$T_{1,optimal}$ (°C)	$m_{1,optimal}$ (kg/s)	$T_{2,optimal}$ (°C)	$\Delta T_{m,1}$ (°C)	$\Delta T_{m,2}$ (°C)	$A_1$ (m <sup>2</sup> )	$A_2$ (m <sup>2</sup> )	$A_{total}$ (m <sup>2</sup> )
196.6	0.350	290.0	194.3	61.5	0.855	0.271	1.126

$$\left\{ \begin{array}{l} Nu = 0.023Re^{0.8}Pr^{0.3}, \text{ when the fluid is being cooled} \\ Nu = 0.023Re^{0.8}Pr^{0.4}, \text{ when the fluid is being heated} \end{array} \right. \quad (27)$$

Fig. 9 depicts the heat transfer area of HEXs in relation to  $m_1$  for a specified intermediate temperature of  $T_1 = 180$  °C. As  $m_1$  increases,  $A_1$  shows a continuous decrease, whereas  $A_2$  exhibits a steady increase. The

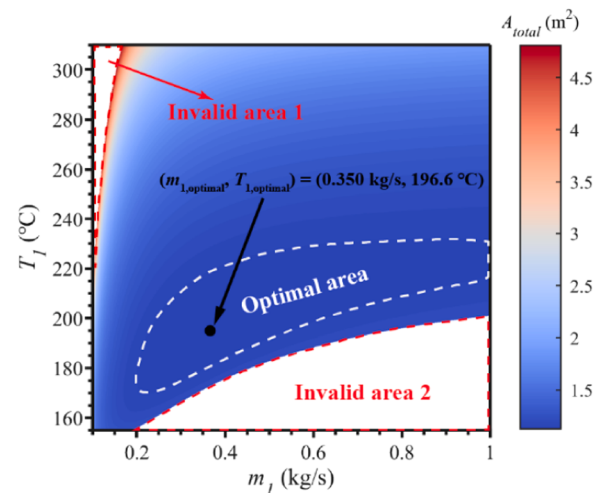


Fig. 14. The distribution of  $A_{total}$  with respect to  $m_1$  and  $T_1$ .

combined influence of  $A_1$  and  $A_2$  produces a non-monotonic pattern in the variation of the  $A_{total}$  as a function of  $m_1$ , initially declining and then rising. This suggests the existence of an optimal value of  $m_1$ , at which the  $A_{total}$  reaches its minimum and thus, results in the system's lightest

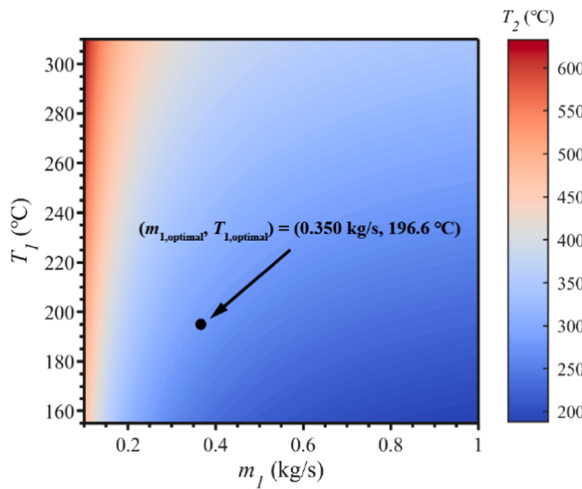


Fig. 15. The distribution of  $T_2$  with respect to  $m_1$  and  $T_1$ .

weight. Fig. 10 illustrates the changes in mean temperature difference across each HEX with respect to  $m_1$  when  $T_1$  is held at 180 °C. Fig. 11 displays the variations of the overall heat transfer coefficient for each HEX, as influenced by changes in  $m_1$ . Given that the heat transfer rate remains constant, increasing  $m_1$  has a positive impact on the cooling air and therefore leads to an increase in  $\Delta T_{m,1}$  for HEX-1. Additionally, as shown in Fig. 11, an increase in  $m_1$  leads to a corresponding rise in  $U_{o,1}$ . The combined effect of these factors causes  $A_1$  to decline monotonically as  $m_1$  increases. Concerning HEX-2, an increase in  $m_1$  leads to a decrease in  $T_2$ , ultimately resulting in a decline of  $\Delta T_{m,2}$ . Although  $U_{o,2}$  slightly increases with  $m_1$ , this growth is limited. The significant factor here is the decrease in  $\Delta T_{m,2}$ , which ultimately results in an increase in  $A_2$  with the increase in  $m_1$ .

In order to examine the impact of a particular intermediate temperature on the optimal  $m_1$ , this study utilizes the aforementioned method to calculate the optimal  $m_1$  and its corresponding  $A_{total}$  for four distinct  $T_1$  values. Table 6 presents the optimal calculation results for  $T_1 \in [180^\circ\text{C}, 230^\circ\text{C}]$ , while Fig. 12 provides a visualization of the variation in HEXs' heat transfer area with respect to  $m_1$  for the four different  $T_1$  values.

It is noteworthy that  $m_{1,optimal}$  increases as the given  $T_1$  increases. This trend can be attributed to the fact that, for HEX-1, a higher  $T_1$  is not conducive to cooling air. Thus, to reduce the design heat transfer area of HEX under a certain heat transfer rate requirement, the mass flow rate of

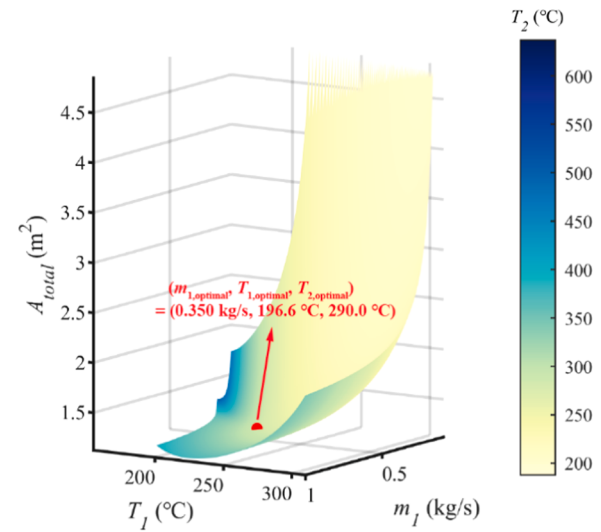


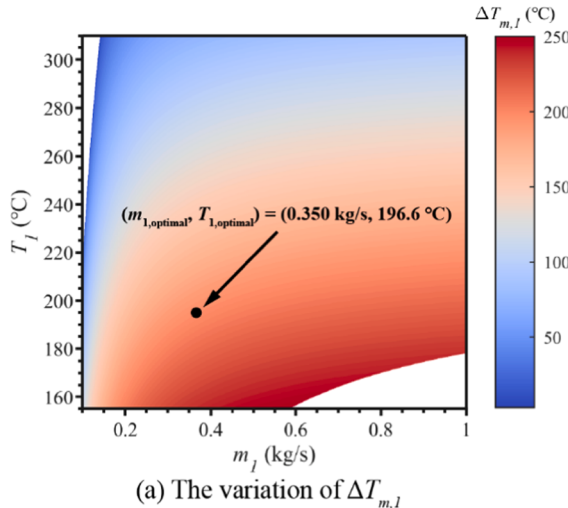
Fig. 17. The three-dimensional distribution of  $A_{total}$  based on  $m_1$  and  $T_1$ .

the cold source (i.e.  $m_1$ ) needs to be increased. Conversely, for HEX-2, a higher  $T_1$  is more beneficial for preheating the fuel. Additionally, Fig. 13 shows that  $\Delta T_{m,2}$  decreases more slowly as  $m_1$  increases, resulting in a slower increase in  $A_2$  with respect to  $m_1$  for larger  $T_1$ . These combined factors lead to a higher optimal IWF mass flow rate for larger  $T_1$ . However, the variation of  $A_{total}$  around the  $m_{1,optimal}$  becomes small as  $T_1$  increases. For instance, when  $T_1$  is 220 °C, the  $A_{total}$  range from 1.142 m<sup>2</sup> to 1.146 m<sup>2</sup> as  $m_1$  varies within ±20% of  $m_{1,optimal}$  (i.e.  $m_1 \in [0.490 \text{ kg/s}, 0.736 \text{ kg/s}]$ ), with a maximum deviation of only 0.35%. This suggests that when  $T_1$  is high, a relatively wide range of  $m_1$  can be selected as the design point without significantly affecting the  $A_{total}$ .

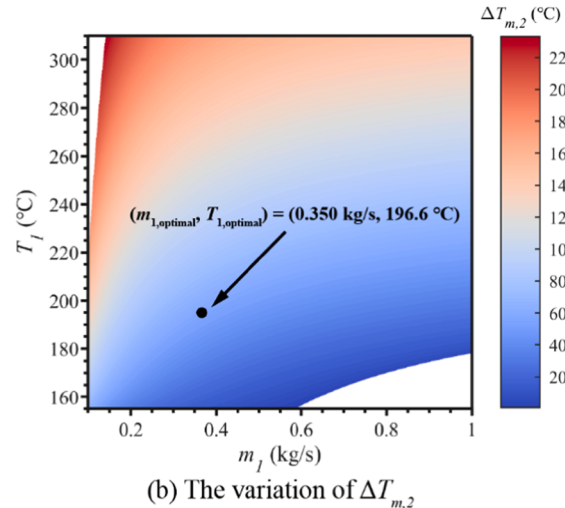
#### 4.3. Results of Case C - $T_1$ and $m_1$ are variable

Table 7 presents the optimum design conditions that minimize the  $A_{total}$  when both  $T_1$  and  $m_1$  are variable. The structure parameters of each HEX are the same as in Table 5. By incorporating the performance of the HEXs with the boundary conditions of the three working fluids, set  $h_{o,1} = 750 \text{ W/m}^2/\text{K}$ ,  $h_{o,2} = 8000 \text{ W/m}^2/\text{K}$ ,  $m_1 \in [0.1 \text{ kg/s}, 1 \text{ kg/s}]$ , and  $T_1 \in [155^\circ\text{C}, 310^\circ\text{C}]$ .

The algorithm outlined in Section 3.5 is employed to determine the optimal point  $(m_{1,optimal}, T_{1,optimal})$  for the system, which is found to be  $(0.350 \text{ kg/s}, 196.6^\circ\text{C})$ . The corresponding minimum  $A_{total}$  is calculated



(a) The variation of  $\Delta T_{m,1}$



(b) The variation of  $\Delta T_{m,2}$

Fig. 16. The distribution of  $\Delta T_{m,1}$  and  $\Delta T_{m,2}$  with respect to  $m_1$  and  $T_1$ .

to be  $1.126 \text{ m}^2$ , with heat exchange unit tube lengths ( $L$ ) of  $2.03 \text{ m}$  for HEX-1 and  $0.75 \text{ m}$  for HEX-2. The tube diameters and numbers are detailed in [Table 5](#). As described in [Section 4.2](#), the inner tube heat transfer coefficient  $h_i$  is calculated using the same methodology. In order to verify the accuracy of the algorithm, a traversal calculation is performed to solve the objective function [Eq. \(25\)](#). Specifically,  $m_1$  and  $T_1$  are divided into 1000 equal intervals within their respective ranges, resulting in a total of  $10^6$  distinct points, and  $A_{total}$  values are calculated at all of these points. However, in order to ensure that each computation point satisfies the nonlinear constraint given by [Eq. \(26\)](#), any point that does not satisfy this condition is assigned an  $A_{total}$  value of NaN (Not a Number). Additionally, to expedite the calculation, any point where the mean average temperature difference of the HEX is less than  $35^\circ\text{C}$  is also assigned an  $A_{total}$  value of NaN since the  $A_{total}$  value corresponding to this point must be large, not the minimum value. The proposed algorithm's accuracy has been confirmed by the minimum value of  $A_{total}$ , which is determined to be  $1.126 \text{ m}^2$  at an optimal point of  $(m_{1,optimal}, T_{1,optimal}) = (0.350 \text{ kg/s}, 196.6^\circ\text{C})$ , obtained through the traversal calculation process. This demonstrates that the algorithm is reliable and can effectively optimize the heat transfer area of HEXs. The detailed results of the optimization calculation are presented in [Table 8](#).

[Fig. 14](#) illustrates the distribution of  $A_{total}$  concerning  $m_1$  and  $T_1$ . However, it is observed that two regions are invalid in the figure, where there are no corresponding  $A_{total}$  values for the calculated points  $(m_1, T_1)$ . The reason for this phenomenon is that the computational points do not satisfy the nonlinear constraints in these regions. This situation can be explained more explicitly through the distribution of  $T_2$ ,  $\Delta T_{m,1}$  and  $\Delta T_{m,2}$  based on  $m_1$  and  $T_1$ , as illustrated in [Fig. 15](#) and [Fig. 16](#), respectively. Invalid area 1 in [Fig. 14](#) is attributed to the fact that the value of  $T_2$  is higher than  $T_{a,i}$ , which implies that the temperature of IWF exceeds the heat source of the entire system, thereby violating the first law of thermodynamics, and is hence discarded. As for the invalid area 2, on one hand, the value of  $T_2$  is lower than  $T_{f,o}$ , which indicates that for HEX-2, the heat source's inlet temperature is lower than the cold source's outlet temperature, which violates the first law of thermodynamics and is consequently discarded. On the other hand, the value of  $\Delta T_{m,2}$  is lower than  $35^\circ\text{C}$ , which does not fulfill the calculation conditions described earlier and is therefore also discarded. [Fig. 17](#) demonstrates the three-dimensional distribution of  $A_{total}$  based on  $m_1$  and  $T_1$ . In this figure, the z-axis corresponds to the value of  $A_{total}$  of the point  $(m_1, T_1)$  among all the calculation results. The values of  $T_2$  are depicted through color contours. The lowest valley of  $A_{total}$  locates on the point  $(m_{1,optimal}, T_{1,optimal}, T_{2,optimal}) = (0.350 \text{ kg/s}, 196.6^\circ\text{C}, 290.0^\circ\text{C})$  with a corresponding optimal  $A_{total}$  of  $1.126 \text{ m}^2$ . Combined with [Fig. 14](#), it can be found that there exists an optimal area where the values of  $A_{total}$  are very low and do not differ much with each point. Similar to the case in [Section 4.2](#), this suggests that the design point of IWF in the intermediate heat exchange cycle system can be selected in the optimal region according to the actual aero engine operating conditions without significantly affecting the  $A_{total}$ .

## 5. Conclusion

The present study constructs an intermediate heat-exchange cycle system of aero engines, which can be applied to the PTCC engines and promote the application of the CCA technology. A novel and convenient approach to determining the IWF mass flow rate and intermediate operating temperature relative to the minimum total heat transfer area is proposed. A two-stage HEX combined intermediate heat-exchange cycle system with Chinese aviation kerosene RP-3 as the fuel and high-pressure water as the IWF is taken as an example to verify the analytical results through numerical calculation. The influence of working conditions on systematic heat transportation is also investigated based on the example. The key findings can be summarized as follows.

- 1) For three different given conditions of mass flow rate and intermediate operating temperature of IWF, there all exists the optimal parameter of IWF where the value of  $A_{total}$  is the minimum corresponding to the minimum system weight.
- 2) The deviation between the analytical results and numerical calculations is found to be reasonably small, at below 0.03%. This demonstrates the validity of the newly proposed approach, which provides a formula or calculation algorithm for determining the optimal parameters of IWF. The proposed approach is shown to be both efficient and convenient, providing an effective alternative for optimizing IWF parameters.
- 3) For the situation of fixed IWF mass flow rate, as the given  $m_1$  increases,  $T_{1,optimal}$  also increases. For the situation of fixed  $T_1$ ,  $m_{1,optimal}$  increases as the given  $T_1$  increases. However, when the given  $T_1$  is high, a relatively wide range of  $m_1$  can be selected as the design point without significantly affecting the  $A_{total}$ . For instance, when  $T_1$  is  $220^\circ\text{C}$ , the  $A_{total}$  range from  $1.142 \text{ m}^2$  to  $1.146 \text{ m}^2$  as  $m_1$  varies within  $\pm 20\%$  of  $m_{1,optimal}$ , with a maximum deviation of only 0.35%.
- 4) For the situation where both  $T_1$  and  $m_1$  are variable, the proposed approach can accurately and quickly calculate the optimal point  $(m_{1,optimal}, T_{1,optimal})$  of IWF. For Case C, the minimum  $A_{total}$  is calculated to be  $1.126 \text{ m}^2$ , with  $L_1 = 2.03 \text{ m}$ ,  $d_{i,1} = 1.4 \text{ mm}$ ,  $d_{o,1} = 1.8 \text{ mm}$ ,  $N_{tube,1} = 96$  for HEX-1 and  $L_2 = 0.75 \text{ m}$ ,  $d_{i,2} = 1.2 \text{ mm}$ ,  $d_{o,2} = 1.6 \text{ mm}$ ,  $N_{tube,2} = 96$  for HEX-2. Moreover, there exists an optimal area where the values of  $A_{total}$  are very low and do not differ much with each point. Therefore, the design parameter points of IWF can be selected in this optimal area according to the actual aero engine operating conditions without significantly affecting the  $A_{total}$ .

## Declaration of generative AI and AI-assisted technologies in the writing process

During the preparation of this work, the authors used Youdao AIBox in order to improve language and readability. After using this tool, the authors reviewed and edited the content as needed and took full responsibility for the content of the publication.

## CRediT authorship contribution statement

**Yanchen Fu:** Methodology, Writing – review & editing, Funding acquisition. **Weitong Liu:** Formal analysis, Investigation, Data curation, Writing – original draft. **Han Qi:** Resources. **Qun Chen:** Writing – review & editing. **Jie Wen:** Supervision. **Guoqiang Xu:** Conceptualization, Project administration.

## Declaration of Competing Interest

The authors declared that they have no conflicts of interest to this work.

## Data availability

Data will be made available on request.

## Acknowledgment

The authors appreciate the supports from the National Science and Technology Major Project of China (Nos. J2019-III-0021-0065 and J2019-III-0015-0059), the Fundamental Research Funds for the Central Universities (Nos 501QYZX2023146001 and 501XTCX2023146001).

## References

- [1] Z.-g. Wang, Y. Wang, J.-q. Zhang, B.-c. Zhang, Overview of the key technologies of combined cycle engine precooling systems and the advanced applications of micro-channel heat transfer, *Aerospace Science and Technology* 39 (2014) 31–39.
- [2] S. Walker, M. Tang, C. Mamplata, TBCC propulsion for a Mach 6 hypersonic airplane, in: 16th AIAA/DLR/DGLR International Space Planes and Hypersonic Systems and Technologies Conference, 2013, pp. 7238.
- [3] T.T. Zhang, X.T. Yan, W. Huang, X.K. Che, Z.G. Wang, Multidisciplinary design optimization of a wide speed range vehicle with waveride airframe and RBCC engine, *Energy* 235 (2021).
- [4] D. Jian, Z. Qiru, Key technologies for thermodynamic cycle of precooled engines: A review, *Acta Astronautica* 177 (2020) 299–312.
- [5] P. Dong, H. Tang, M. Chen, Study on multi-cycle coupling mechanism of hypersonic precooled combined cycle engine, *Applied Thermal Engineering* 131 (2018) 497–506.
- [6] H. Webber, A. Bond, M. Hempsell, Sensitivity of pre-cooled air-breathing engine performance to heat exchanger design parameters, in: 57th International Astronautical Congress, 2006, pp. D2. P. 2.07.
- [7] R. Welge, N+2 Supersonic Concept Development and Systems Integration., NASA/CR-2010-216842, 2010.
- [8] E. Baltman, J.C. Tai, M. Shi, D.N. Mavris, An Investigation of Cooled Cooling Air for a Mach 2.2 Commercial Supersonic Transport, in: AIAA Propulsion and Energy 2021 Forum, 2021.
- [9] H. Huang, L.J. Spadaccini, D.R. Sobel, Fuel-cooled thermal management for advanced aeroengines, *J. Eng. Gas Turbines Power* 126 (2) (2004) 284–293.
- [10] W. Liu, G. Xu, Y. Fu, J. Wen, N. Zhang, Numerical investigation on forced, natural, and mixed convective heat transfer of n-decane in laminar flow at supercritical pressures, *International Journal of Heat and Mass Transfer* (2023) 209.
- [11] N.R. Herring, S.D. Heister, Review of the development of compact, high performance heat exchangers for gas turbine applications, *ASME International Mechanical Engineering Congress and Exposition* (2006) 467–476.
- [12] B.A. Miller, Analysis of several methane-fueled engine cycles for Mach 3.0 flight, 1968.
- [13] R.J. Boyle, S.M. Jones, Effects of Precooling Turbine Cooling Air on Engine Performance, *Proceedings of Asme Turbo Expo 4* (2009) 495–504, 2009Vol.
- [14] P. Gray, B. Kestner, D. Mavris, Parametric Heat Exchanger Design for Next Generation Advanced Vehicle and Propulsion System Analysis, in: 48th AIAA/ASME/SAE/ASEE Joint Propulsion Conference & Exhibit, 2012.
- [15] L. Zhuang, G. Xu, Q. Liu, M. Li, B. Dong, J. Wen, Superiority analysis of the cooled cooling air technology for low bypass ratio aero-engine under typical flight mission, *Energy Conversion and Management* (2022) 259.
- [16] P. Liu, H. Han, Z. Bao, Multi-objective optimization of fuel-air tube-in-tube helical coil heat exchangers for cooled cooling air system applied in aeroengines, *Aerospace Science and Technology* (2022) 130.
- [17] Z. Tao, Y. Fu, G. Xu, H. Deng, Z. Jia, Experimental Study on Influences of Physical Factors to Supercritical RP-3 Surface and Liquid-Space Thermal Oxidation Coking, *Energ Fuel* 28 (9) (2014) 6098–6106.
- [18] J. Sarkar, S. Bhattacharyya, Overall conductance and heat transfer area minimization of refrigerators and heat pumps with finite heat reservoirs, *Energy Conversion and Management* 48 (3) (2007) 803–808.
- [19] A. Bejan, Entropy generation minimization: The new thermodynamics of finite-size devices and finite-time processes, *Journal of Applied Physics* 79 (3) (1996) 1191–1218.
- [20] J. Wu, A new approach to determining the intermediate temperatures of endoreversible combined cycle power plant corresponding to maximum power, *International Journal of Heat and Mass Transfer* 91 (2015) 150–161.
- [21] Q. Yin, W.-J. Du, L. Cheng, Optimization design of heat recovery systems on rotary kilns using genetic algorithms, *Applied Energy* 202 (2017) 153–168.
- [22] S.-I. Na, M.S. Kim, Y.-J. Baik, M. Kim, Optimal allocation of heat exchangers in a Supercritical carbon dioxide power cycle for waste heat recovery, *Energy Conversion and Management* (2019) 199.
- [23] Y. Song, D. Li, F. Cao, X. Wang, Investigation of the optimal intermediate water temperature in a combined r134a and transcritical CO<sub>2</sub> heat pump for space heating, *International Journal of Refrigeration* 79 (2017) 10–24.
- [24] Y. Song, F. Cao, The evaluation of the optimal medium temperature in a space heating used transcritical air-source CO<sub>2</sub> heat pump with an R134a subcooling device, *Energy Conversion and Management* 166 (2018) 409–423.
- [25] C. Wang, X. Yu, X. Pan, J. Qin, H. Huang, Thermodynamic optimization of the indirect precooled engine cycle using the method of cascade utilization of cold sources, *Energy* 238 (2022).
- [26] L. Chen, F. Sun, C. Wu, Optimal allocation of heat-exchanger area for refrigeration and air-conditioning plants, *Applied Energy* 77 (3) (2004) 339–354.
- [27] K. Thulukkanam, *Heat exchanger design handbook*, CRC press, 2013.
- [28] K. Deb, *Multi-objective optimisation using evolutionary algorithms: an introduction*, Springer, 2011.
- [29] L. Gosselin, M. Tye-Gingras, F. Mathieu-Potvin, Review of utilization of genetic algorithms in heat transfer problems, *International journal of heat and mass transfer* 52 (9-10) (2009) 2169–2188.
- [30] D. Pham, D. Karaboga, *Intelligent optimisation techniques: genetic algorithms, tabu search, simulated annealing and neural networks*, Springer Science & Business Media, 2012.
- [31] Q. Liu, G. Xu, J. Wen, Y. Fu, L. Zhuang, B. Dong, Multivariate Design and Analysis of Aircraft Heat Exchanger Under Multiple Working Conditions Within Flight Envelope, *Journal of Thermal Science and Engineering Applications* 14 (6) (2022).
- [32] T. Selleri, B. Najafi, F. Rinaldi, G. Colombo, Mathematical modeling and multi-objective optimization of a mini-channel heat exchanger via genetic algorithm, *Journal of Thermal Science and Engineering Applications* 5 (3) (2013).
- [33] J.Y. Wong, S. Sharma, G. Rangaiah, Design of shell-and-tube heat exchangers for multiple objectives using elitist non-dominated sorting genetic algorithm with termination criteria, *Applied Thermal Engineering* 93 (2016) 888–899.
- [34] The MathWorks Inc, MATLAB version: 9.11.0 (R2021b), The MathWorks Inc., Natick, Massachusetts, 2021.
- [35] I.H. Bell, J. Wronski, S. Quoilin, V. Lemort, Pure and Pseudo-pure Fluid Thermophysical Property Evaluation and the Open-Source Thermophysical Property Library CoolProp, *Ind Eng Chem Res* 53 (6) (2014) 2498–2508.
- [36] H. Deng, C. Zhang, G. Xu, Z. Tao, B. Zhang, G. Liu, Density measurements of endothermic hydrocarbon fuel at sub-and supercritical conditions, *Journal of Chemical & Engineering Data* 56 (6) (2011) 2980–2986.
- [37] H. Deng, C. Zhang, G. Xu, B. Zhang, Z. Tao, K. Zhu, Viscosity measurements of endothermic hydrocarbon fuel from (298 to 788) K under supercritical pressure conditions, *Journal of Chemical & Engineering Data* 57 (2) (2012) 358–365.
- [38] H. Deng, K. Zhu, G. Xu, Z. Tao, C. Zhang, G. Liu, Isobaric specific heat capacity measurement for kerosene RP-3 in the near-critical and supercritical regions, *Journal of Chemical & Engineering Data* 57 (2) (2012) 263–268.
- [39] G. Xu, Z. Jia, J. Wen, H. Deng, Y. Fu, Thermal-conductivity measurements of aviation kerosene RP-3 from (285 to 513) K at sub-and supercritical pressures, *International Journal of Thermophysics* 36 (4) (2015) 620–632.
- [40] Y. Liu, G. Xu, Y. Fu, J. Wen, S. Qi, L. Lyu, Airside pressure drop characteristics of three analogous serpentine tube heat exchangers considering heat transfer for aero-engine cooling, *Chinese Journal of Aeronautics* 35 (12) (2022) 32–46.
- [41] A. Bejan, *Convection heat transfer*, John Wiley & Sons, 2013.